Original scientific paper
https://doi.org/10.33180/InfMIDEM2024.306

Informacije MIDEM
Journal of Microelectronics, Electronic Components and Materials
Vol. 54, No. 3(2024), 225 – 233

Cold Sintering of Perovskite–Perovskite Particulate Composite Based on $K_{0.5}Na_{0.5}NbO_3$ and $BiFeO_3$

Samir Salmanov[1,2], Danjela Kuščer[1,2], Mojca Otoničar[1,2]

[1]Electronic Ceramics Department, Jožef Stefan Institute, Ljubljana, Slovenia
[2]Jožef Stefan International Postgraduate School, Ljubljana, Slovenia

Abstract: The cosintering of particulate composites often presents a challenge due to the conventionally high processing temperatures used. Inter-diffusion of species between two phases and their volatilization, formation of secondary phases, and cracking or delamination of ceramics are effects that hinder the coupling of functional properties and reduce the final responses of such composites. This is particularly relevant when producing perovskite–perovskite composites from phases that are conventionally sintered at different temperatures (Ts), such as $K_{0.5}Na_{0.5}NbO_3$ (KNN; Ts≈1100 °C) and $BiFeO_3$ (BFO; Ts≈800 °C). Obtaining high-quality KNN–BFO multifunctional composite was the goal of this study. We demonstrate herein that the low-temperature sintering technique known as the Cold Sintering Process (CSP) can be utilized for producing particulate perovskite–perovskite composites, specifically KNN–BFO. We show that cold-sintered KNN–BFO composites have a dense microstructure, good phase-to-phase contact, are crack-free and exhibit ferroelectric properties. Their dielectric and ferroelectric properties are strongly affected by the fraction of KNN, increasing polarization saturation, while BFO aids in increasing their dielectric breakdown strength.

Keywords: cold sintering process; ferroelectric; particulate composite; $BiFeO_3$; $K_{0.5}Na_{0.5}NbO_3$

Hladno sintranje prahov perovskitov na osnovi $K_{0.5}Na_{0.5}NbO_3$ in $BiFeO_3$

Izvleček: Sosintranje dveh različnih praškastih keramičnih materialov v kompozitne strukture predstavlja izziv, saj keramika zahteva pripravo pri visokih temperaturah. Pri teh pogojih, difuzija ionov med dvema fazama, sublimacija, tvorba sekundarnih faz ter nastanek razpok ali delaminacija keramike vplivajo na lastnosti kompozita in poslabšajo njegove funkcijske lastnosti. To je še posebej pomembno pri izdelavi kompozitov iz dveh perovskitnih faz, ki se običajno sintrajo pri različnih temperaturah (Ts). Tak primer so kompoziti na osnovi $K_{0.5}Na_{0.5}NbO_3$ (KNN; Ts≈1100 °C) in $BiFeO_3$ (BFO; Ts≈800 °C) feroelektričnih sestav, KNN-BFO, katerih pripravo in lastnosti obravnava ta študija. Dokazali smo, da je mogoče tehniko nizkotemperaturnega sintranja, znano kot postopek hladnega sintranja (CSP), uporabiti za izdelavo kompozitov iz prahov dveh različnih feroelektričnih perovskitnih materialov, KNN in BFO. Pokazali smo, da imajo hladno sintrani kompoziti gosto mikrostrukturo, dober stik med fazami, so brez razpok in izkazujejo feroelektrični odziv. Na povišanje dielektričnih in feroelektričnih lastnosti močno vpliva delež KNN v kompozitu, ki povečuje polarizacijsko nasičenost, medtem ko BFO pripomore k povečanju njihove dielektrične prebojne trdnosti.

Ključne besede: hladno sintranje; feroelektriki; kompozit; $BiFeO_3$; $K_{0.5}Na_{0.5}NbO_3$

** Corresponding Author's e-mail: samir.salmanov@ijs.si*

1 Introduction

Ferroelectric perovskites are widely used in a variety of electronic devices such as capacitors, sensors, actuators, and transducers [1]. Among environmentally friendly lead-free materials, $K_{0.5}Na_{0.5}NbO_3$ (KNN) is a suitable candidate to replace $Pb(Zr_{1-x}Tix)O_3$ (PZT) in piezoelectric applications, and $BiFeO_3$ (BFO) [2]–[4] is widely investigated and used for multiferroic coupling or high-temperature piezoelectric applications. Combination of the two functional materials in the form of a multiferroic composites with properties that can be fine-tuned by adjusting amounts of each individual

How to cite:
S. Salmanov et al., "Cold Sintering of Perovskite–Perovskite Particulate Composite Based on $K_{0.5}Na_{0.5}NbO_3$ and $BiFeO_3$", Inf. Midem-J. Microelectron. Electron. Compon. Mater., Vol. 54, No. 3(2024), pp. 225–233

phase could be beneficial for use in electronic devices, integrated as a single multifunctional component [5].

However, processing of perovskite-perovskite particulate composites by a conventional cosintering route is challenging due to different sintering temperatures of materials of different composition, volatilization of elements and their diffusion coefficients. In the case of KNN and BFO ceramics, KNN densifies in a narrow temperature range at ~1100 °C, close to its melting point of 1140 °C [2], while BFO densifies at ~300 °C lower temperature of 800 °C. Above ~950 °C BFO decomposes into liquid phase and Fe-rich phase and is fully melted at 1100 °C [4], [6]–[8]. It was also reported that cosintering of KNN and $BaFe_{12}O_{19}$ at 1125 °C led to volatilization of alkalies, resulting in decreased relative density of the composite [9]. It was further demonstrated for $CoFe_2O_4$ (CFO) and PZT composite that Fe^{3+} can diffuse into PZT, and Ti^{4+} can diffuse into CFO already at 900–1000 °C [10]–[12]. This diffusion facilitates secondary phase formation, limiting functional-property coupling between the two phases, and can cause creation of oxygen vacancies, leading to enhanced conductivity of the composite [10]. In an attempt to limit such diffusion, in the case of cosintering of BFO and $BaTiO_3$ [13], as well as BFO and PZT [14], low sintering temperatures were used, but the microstructure was highly porous.

Beside the different sintering temperatures of the composite phases and with that the possible interdiffusion of species between the two phases during cosintering, forming a third solid-solution phase, producing composites is challenging also due to different thermal expansion coefficient (TEC) of individual phases. The latter may cause strains at the interfaces of different phases and microcracks [15], [16] during cooling of the composite from the processing temperature due to different shrinkage parameters of the lattices. The cracking effect due to different TEC of two composite phases is more evident in the case of a layered composite structure, e.g., cosintering CFO and PZT in a sandwiched structure resulted in cracks along the interface and delamination or the structure [17]. On the other hand, it was shown for CFO–PZT [18] and Co-doped BFO–PZT composite [12], as well as in the co-sintered BFO–$Ni_{0.5}Co_{0.5-x}Zn_xFe_2O_4$ composite [19] that interfacial strains influence the lattice distortions of individual phases, contributing to large magnetoelectric coupling. In the case of materials of our interest, BFO and KNN, BFO has TEC of 10.9 $x10^{-6}$ K^{-1} and 12.2$x10^{-6}$ K^{-1} for the temperature range 25–325 °C and 344–838 °C, respectively [20], while KNN has TEC of 2.96$x10^{-6}$ K^{-1}, 4.35$x10^{-6}$ K^{-1} and 7.52 $x10^{-6}$ K^{-1} for the temperature range 30–195 °C, 208–364 °C and 434–790 °C, respectively [21]. This implies that BFO will shrink almost twice more than KNN when cooling down from the sintering temperature, likely producing strains at the interfaces and/or cracks.

A way to severely limit thermal expansion/shrinkage, diffusion or volatilization of species during sintering of composites is to sinter at temperatures below 300 °C. Cold sintering process (CSP) is a sintering technique that allows densification of materials at temperatures even below 300 °C, under applied uniaxial pressure of a few hundreds of MPa and in the presence of a transient liquid phase, which facilitates material densification through a pressure-dissolution process [22]. The low processing temperature of the CSP provides opportunities for combining a variety of materials, i.e., ceramic with polymers or metals, as well as different types of oxides [23]–[27]. While different perovskites have been cold-sintered so far, including KNN-based compositions and BFO ceramics [28], there are no reports yet on cold sintering of perovskite-perovskite composites, which is a viable way to produce multifunctional components.

In this contribution we studied the processing of KNN–BFO perovskite-perovskite particulate composite with different ratios of phases, using the CSP. Based on our previous investigations on cold sintering of KNN [29], [30] and BFO [28], we utilized a eutectic mixture of NaOH and KOH as a transient liquid phase (TLP) to aid the sintering of the composite, which resulted in a homogeneous distribution of the two phases, no secondary phases formed at the grain boundaries, and a dense microstructure. The aim of our work is to illustrate that cold sintering can be successfully employed for combining two ferroelectric perovskite compositions to produce high-quality composites as multifunctional components.

2 Materials and methods

The initial powder compositions, $BiFeO_3$ with added 0.1 wt.% Co (named BFO hereafter), and $K_{0.5}Na_{0.5}NbO_3$ (KNN), were prepared via solid-state synthesis. Details on preparation can be found elsewhere (KNN powder was calcined at 850 °C) [31], [32]. Both powders were separately milled at 200 rpm for 0.5h (KNN) and 2h (BFO) after calcination to break the agglomerates. The mean particle of KNN was d_{50} = 0.50 µm and for BFO d_{50} = 1.39 µm. Different ratios of KNN and BFO powders were then mixed together in an agate mortar to produce (1-x)KNN–xBFO compositions with x= 0, 0.33, 0.50 and 0.66 and 1 (in weight fraction). The samples are denoted as: KNN, 33%BFO, 50%BFO, 66%BFO and BFO, respectively. Converting BFO weight % into volume %, the three compositions are 20%BFO, 35%BFO and

50%BFO, respectively. For each composition, 75 µl of NaOH-KOH aqueous equimolar mixture was added to 0.6 g of powders and manually mixed in an agate mortar. The NaOH-KOH solution was prepared by dissolving NaOH (molarity is 4.26 M) and KOH (molarity is 4.26 M) in water. The moist powders were put in the CSP instrument and pressed under 676 MPa uniaxial pressure (with a pressing rate of 13 MPa/minute) and heated to 300 °C (with heating and cooling rates of 2 K/min) and cold-sintered for 2 hours. The slow rates have previously been shown to produce reliable crack-free samples [33] and were chosen here for two reasons, one being better liquid/particle distribution in the green compact and the other being the polymorphic phase transition at about 170 °C for KNN which might cause large strains due to lattice volume changes and cracking of grains/pellet. After CSP, the obtained pellets with thickness ~1.8 mm and diameter of 8 mm were dried in vacuum drier at 80 °C overnight. Microstructure analysis of cold-sintered samples was performed on polished samples using a scanning electron microscope using backscattered electrons (SEM; JSM 7600 F, Jeol Ltd., Tokyo, Japan). Relative density of cold-sintered samples was calculated based on measured porosity from several SEM images. For dielectric and ferroelectric measurements, the samples were thinned to 0.15-0.25 mm, and gold-sputtered on both sides (using sputtering system 5Pascal, Italy). Dielectric properties were measured with an LCR meter (Hewlett Packard, Tokyo, Japan). Ferroelectric properties (polarization vs. electric field) were measured with a TF2000 analyzer (AixACCT Systems GmbH, Aachen, Germany) at a frequency of 100 Hz with a sinusoidal voltage waveform until their breakdown. Selected samples were annealed in O_2 flow at 500 °C for 2 hours, with 2 K/min heating and cooling rates for dielectric measurements.

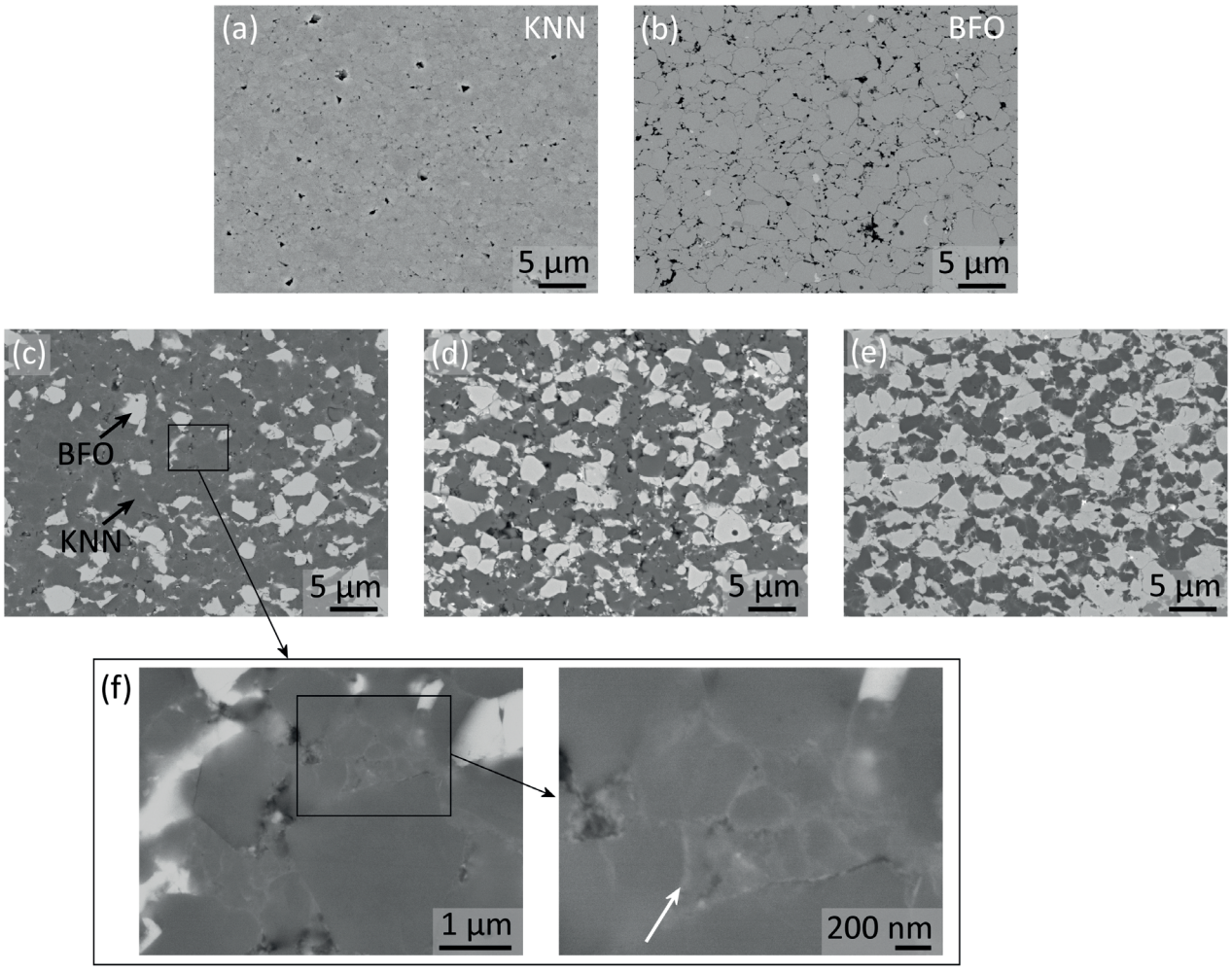

Figure 1: SEM images of ceramic samples cold sintered at 300 °C for 2 hours at 635 MPa with NaOH–KOH as a transient liquid phase: (a) KNN; (b) BFO; (c) 33%BFO; (d) 50%BFO and (e) 66%BFO (percentage given in wt.%). Light grey color of grains in the composites is BFO, and dark grey color of grains is KNN for (c), (d) and (e). Black spots are pores. (f) Enlarged area from 33%BFO composite in (c), showing grain-boundary contacts between KNN grains (white arrow in the right image).

3 Results and discussion

The microstructures of cold-sintered KNN–BFO composites with compositions 33%BFO, 50%BFO and 66%BFO, as well as single-phase KNN and BFO for comparison, are presented in Figure 1. The average grain size of KNN is about 1 µm or less, while BFO has larger grains, ranging up to 5 µm. No secondary phases are observed at the grain boundaries in KNN and BFO from the cold sintering procedure (Figure 1a-b). KNN shows higher relative density compared to BFO, with estimated 98 % compared to 94 %, respectively. Such a difference could be related to several reasons, one being better particle packing in KNN due to smaller initial particles. On the other hand, higher density of cold-sintered KNN compared to BFO can also be explained by the different levels of solubility of each ceramic in the base solution and/or eutectic liquid phase. It was previously shown for KNN dipped in aqueous solution of NaOH that the concentration of Nb^{5+} ions starts to increase already at 50 °C [34], indicating its significant solubility. No studies were found for the solubility of BFO, however, it was shown that during its hydrothermal synthesis it was only possible to dissolve and precipitate BFO species at temperatures above 175-200 °C [35]. This may indicate that KNN is more soluble in the NaOH-KOH liquid phase compared to BFO, leading to higher densification levels of KNN during cold sintering. The third argument for better compaction of KNN could be its ability to significantly plastically deform with applied pressure that seems to exceed the yield strength of the material (e.g., for $KNbO_3$ crystal yield strength of 40 to 120 MPa was reported [36], [37]. Finally, the plastic deformation is realized through dislocation formation and lattice gliding [29], [30], [38], which may have been more efficient in KNN due to its lower density and/or weaker chemical bonding, resulting in a denser microstructure of KNN compared to BFO.

Microstructures of KNN–BFO composites (Figure 1c–e) show that KNN (dark grey phase) and BFO (bright grey phase) are homogeneously distributed, and the relative densities of 33%BFO, 50%BFO and 66%BFO, calculated from measured porosity from the microstructures, are ~96 %. Enlarged view of the 33%BFO composite in Figure 1f shows grain-boundary contacts, indicating good adhesion between the KNN grains, creating a matrix, with BFO grains well compacted between the sintered KNN grains.

These boundaries appear to be slightly curved, confirming the pressure-dissolution process [22] during

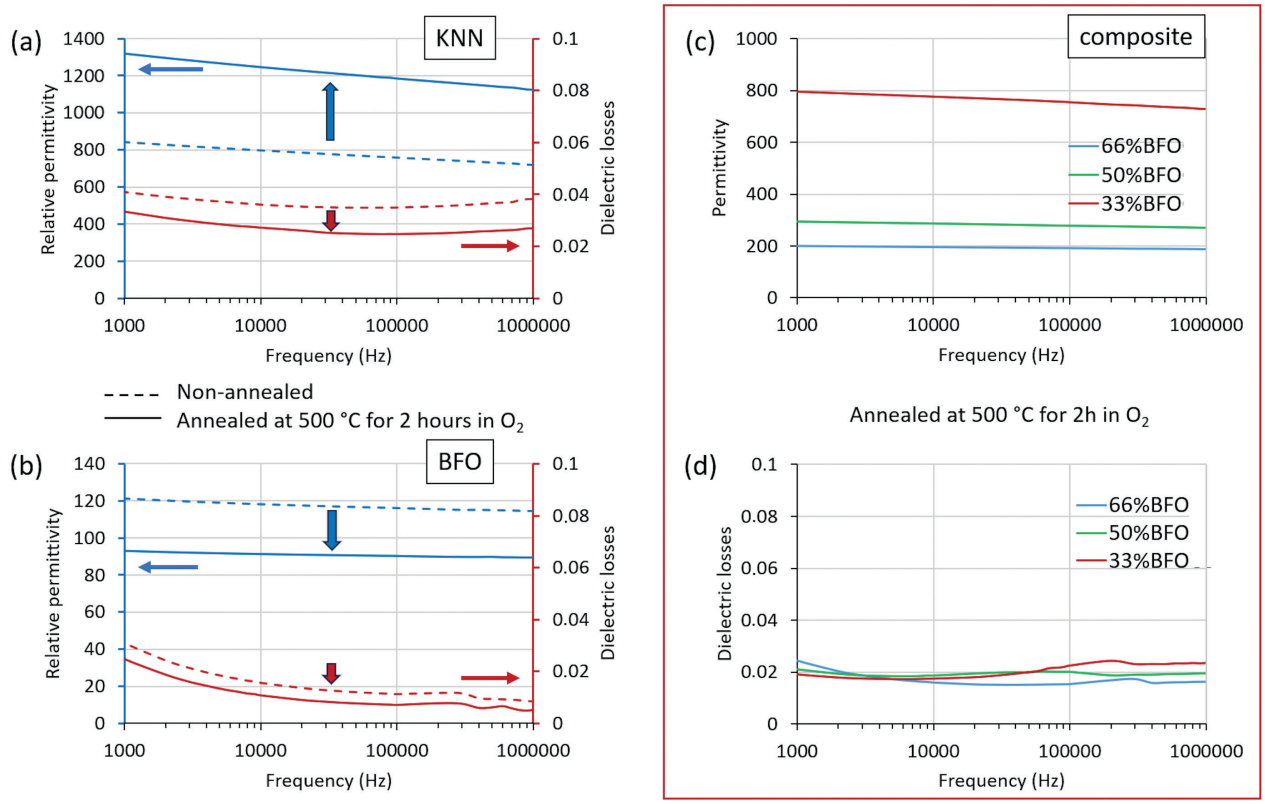

Figure 2: Comparison of dielectric permittivity and dielectric losses of as-prepared cold-sintered samples and samples annealed at 500 °C for 2 hours in O_2 (a) KNN and (b) BFO. (c) and (d) dielectric permittivity and losses of 33%BFO, 50%BFO and 66%BFO composites after annealing

cold sintering, but also appear lighter-grayish, which could indicate a Bi- or Nb-rich phase as a consequence of liquid-phase formation and precipitation of such a phase. The quantity of this phase, however, was too low to be identified by energy dispersive X-ray spectroscopy in SEM or X-ray diffraction. In 50%BFO, and especially in 66%BFO sample, contacts between BFO grains are observed that also show good contact and adhesion. No cracks are seen throughout the composites, which reflects good sintering and adhesion of grains, and minimal thermal expansion of the phases in the temperature range from sintering (300 °C) to room temperature.

The dielectric properties, presented in Figure 2, were measured on the as-prepared and dried cold-sintered KNN, BFO and composite samples, and after O_2 annealing. The as-prepared BFO exhibits the relative dielectric permittivity of ~120 and dielectric losses below 3% in a frequency range from 1 kHz to 1 MHz, and after annealing in O_2 no significant decrease in relative dielectric permittivity and dielectric losses is observed (Figure 2a). The cold-sintered KNN is characterized by a relative dielectric permittivity of ~800 and dielectric losses of 4% in a frequency range from 1 kHz to 1 MHz. However, after annealing in O_2, the dielectric permittivity increased by more than 50 %, while the dielectric losses decreased (Figure 2b). These results are consistent with previous data [30], [39]. The changes in dielectric properties after annealing in O_2 are believed to arise from the reoxidation of the perovskite and changes in the valence states of Nb atom, which was reduced from Nb^{5+} to Nb^{4+} during the CSP. For this reason, composites were also annealed in O_2.

The relative dielectric permittivity and dielectric losses of 33%BFO, 50%BFO and 66%BFO composites after annealing at 500 °C in O_2 are shown in Figure 2c and 2d, respectively. The 66%BFO composite exhibited relative dielectric permittivity of ~200, slightly higher than that of BFO. We can further follow a trend with increasing amount of KNN in the composites, resulting in an increase in the relative dielectric permittivity, with the value for the 33%BFO composite still lower than that of KNN. Especially notable is the difference in relative dielectric permittivity between 33%BFO and 50%BFO compared to the difference between 50%BFO and 33%BFO, which is minimal. This could be related to a critical amount of KNN in the composite. Since in 33%BFO there is only 20 vol. % of BFO, this suggests that the contribution to the relative dielectric permittivity of KNN dominates over BFO. On the other hand, the amount of BFO increases to 35 vol. % and 50 vol. % in 50%BFO and 66%BFO composites, respectively, increasing the contribution of BFO to the dielectric properties, decreasing the relative dielectric permittivity. Interestingly, the values of the dielectric losses of all the composites were similar in the studied frequency range, but slightly higher in the low-frequency range in 66%BFO, similar to pure BFO, which could indicate local conductivity due to defect states in the BFO phase (Figure 2d).

The P–E-loops at 150 kV/cm applied electric field of cold-sintered KNN and BFO and composites 33%BFO, 50%BFO and 66%BFO are shown in Figure 3a. The results show that the coercive field (E_c) and remanent polarization (P_r) values of the composites are between the values for KNN and BFO. 33%BFO and 50%BFO samples show a similar P_r value, while P_r of 66%BFO is smaller, which is in line with the value of the major constituent phase, BFO. The KNN loop shows polarization saturation reached at 150 kV/cm applied, with P_s=30 μC/cm^2. The P–E loop of BFO, however, remains flat at this field and only starts to open at an applied electrical field greater than 150 kV/cm (see inset in Figure 3a for the BFO loop at 200 kV/cm). This indicates defect states in the material that unpin the domains only at stronger fields applied. The effect of defects seems to be hindered in the case of composites with increasing KNN phase, increasing also the P_r value. On the other hand, dielectric breakdown strength seems to be strongly affected by the amount of BFO in the composite, increasing the maximum possible applied electric field (E_{max}) (Figure 3b). We note here that while we did not systematically measure the dielectric breakdown strength of these materials, we consistently observe for all cold-sintered perovskites that the samples withstand larger electrical fields applied without their dielectric breakdown. The final reached value of P_r of the composite seems to be affected by the strength of the grain-boundary contacts between the KNN grains (see enlarged view in Figure 1f), which are more frequent in the composite with larger KNN amount. The analysis of the evolution of P–E loops with gradually increasing electric field for composites (Figure 3c–e) shows that in 66%BFO at maximum applied field (see the loop at 170 kV/cm) the P–E loop starts to open and becomes more rounded. This indicates a major contribution to electrical properties from the BFO phase with unpinning of defects and increased conductivity [31]. Comparison of the functional properties of cold-sintered samples is summarized in Table 1.

4 Conclusions

We demonstrated that CSP can be effectively utilized for sintering of perovskite–perovskite particulate composites based on different ratios of KNN and BFO. Microstructure analysis revealed that the composites have a

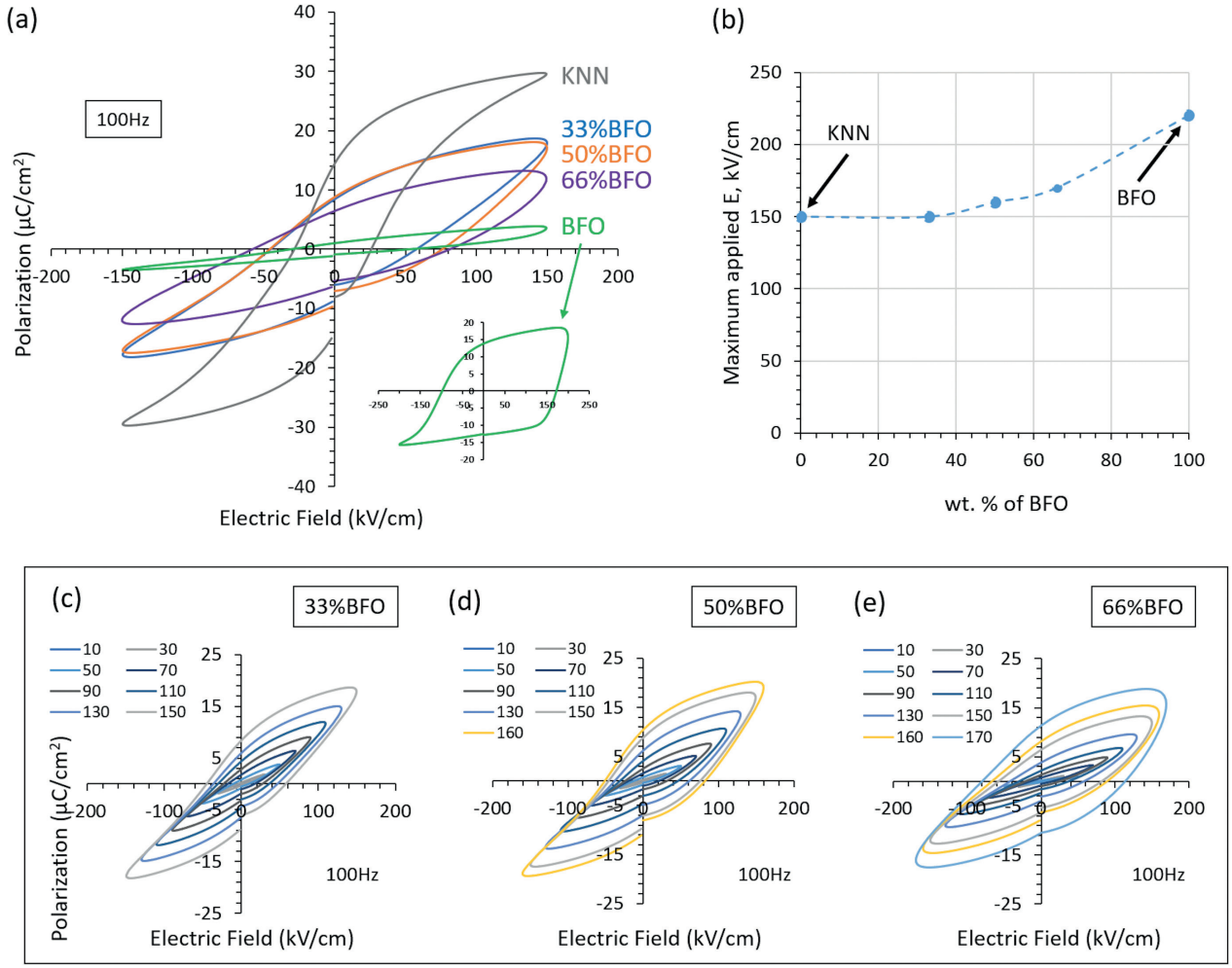

Figure 3: Comparison of ferroelectric properties cold-sintered KNN, BFO and composite ceramics after annealing 500 °C for 2 hours in O2. (a) Polarization–electric-field (P–E) loops at 150 kV/cm. Inset shows the P–E loop of BFO at 200 kV/cm. (b) Maximum applied electric field during measurement of P–E loops for all samples before breakdown. (c)–(e) Evolution of P–E loops with increasing E for (c) 33%BFO, (d) 50%BFO and (e) 66%BFO composites. All measurements were done at 100 Hz

dense structure and homogeneously distributed KNN and BFO grains. Moreover, the contact regions between KNN and BFO grains did not exhibit any cracks or large pores, nor significant secondary phases. After annealing in O_2, the dielectric losses were below 3% across the entire frequency range of 1 kHz to 1 MHz and the values of relative dielectric permittivity were in line with ~~KNN~~ amount of KNN, increasing with increasing KNN fraction. Nevertheless, the composite with 66 wt. % of BFO, where the contacts between KNN grains are rare, demonstrated approximately two times higher permittivity that single-phase cold-sintered BFO, and similar dielectric loss values. The composites showed decent ferroelectric properties and increasing polarization saturation with KNN content, while dielectric breakdown strength appeared higher with increasing BFO content. Remanent polarization is also enhanced by larger KNN fraction when up to 150 kV/cm field is applied, while

Table 1: Comparison of functional properties of cold-sintered samples

	Permittivity at 1kHz	Dielectric losses at 1kHz	Pr at 150 kV/cm	Pr at 200 kV/cm	Emax, kV/cm
KNN	~1300	~0.03	~14	-	150
33%BFO	~800	~0.02	~8	-	150
50%BFO	~300	~0.02	~8	-	160
66%BFO	~200	~0.02	~6	-	170
BFO	~100	~0.02	~2	~14	220

larger fraction of BFO in the composite allows to apply fields above 150 kV/cm, apparently increasing the breakdown strength of the composite.

5 Acknowledgments

The authors acknowledge the help of Brigita Kmet for KNN powder synthesis, Electronic Ceramics Department, Jožef Stefan Institute. The authors acknowledge the financial support of the Slovenian Research and Innovation Agency (core funding J2-2508, J2-50077, program P2-0105).

6 Conflict of Interest

The authors declare no conflict of interest.

7 References

1. G. H. Haertling, "Ferroelectric ceramics: history and technology," *J. Am. Ceram. Soc.*, vol. 82, no. 4, pp. 797–818, Apr. 1999, https://doi.org/10.1111/j.1151-2916.1999.tb01840.x.
2. B. Malič *et al.*, "Sintering of lead-free piezoelectric sodium potassium niobate ceramics," *Materials (Basel).*, vol. 8, no. 12, pp. 8117–8146, Dec. 2015, https://doi.org/10.3390/ma8125449.
3. K. Hui *et al.*, "KNN based high dielectric constant X9R ceramics with fine grain structure and energy storage ability," *J. Am. Ceram. Soc.*, vol. 104, no. 11, pp. 5815–5825, Nov. 2021, https://doi.org/10.1111/jace.17970.
4. T. Rojac *et al.*, "BiFeO 3 Ceramics: Processing, Electrical, and Electromechanical Properties," *J. Am. Ceram. Soc.*, vol. 97, no. 7, pp. 1993–2011, Jul. 2014, https://doi.org/10.1111/jace.12982.
5. N. Ortega, A. Kumar, J. F. Scott, and R. S. Katiyar, "Multifunctional magnetoelectric materials for device applications," *J. Phys. Condens. Matter*, vol. 27, no. 50, p. 504002, Dec. 2015, https://doi.org/10.1088/0953-8984/27/50/504002.
6. M. I. Morozov, N. A. Lomanova, and V. V. Gusarov, "Specific features of BiFeO3 formation in a mixture of bismuth(III) and iron(III) oxides," *Russ. J. Gen. Chem.*, vol. 73, no. 11, pp. 1676–1680, Nov. 2003, https://doi.org/10.1023/B:RUGC.0000018640.30953.70.
7. R. Palai *et al.*, "β phase and γ–β metal-insulator transition in multiferroic BiFeO3," *Phys. Rev. B*, vol. 77, no. 1, p. 014110, Jan. 2008, https://doi.org/10.1103/PhysRevB.77.014110.
8. M. S. Bernardo, "Synthesis, microstructure and properties of BiFeO3-based multiferroic materials: A review," *Boletín la Soc. Española Cerámica y Vidr.*, vol. 53, no. 1, pp. 1–14, Feb. 2014, https://doi.org/10.3989/cyv.12014.
9. P. Kasaeipoor Naeini, T. Delshad Chermahin, M. Shayegh Boroujeny, B. Ebadzadeh, M. Nilforoushan, and M. Abdollahi, "Study of dielectric properties of lead-free multiferroic KNN/22.5 BaFe12O19 composites," *Adv. Ceram. Prog.*, vol. 7, no. 3, pp. 23–28, 2021, https://doi.org/10.30501/ACP.2021.298611.1071.
10. S. Basu, K. R. Babu, and R. N. P. Choudhary, "Studies on the piezoelectric and magnetostrictive phase distribution in lead zirconate titanate–cobalt iron oxide composites," *Mater. Chem. Phys.*, vol. 132, no. 2–3, pp. 570–580, Feb. 2012, https://doi.org/10.1016/j.matchemphys.2011.11.071.
11. P. Jenus, D. Lisjak, D. Kuscer, D. Makovec, and M. Drofenik, "The low-temperature cosintering of cobalt ferrite and lead zirconate titanate ceramic composites," *J. Am. Ceram. Soc.*, vol. 97, no. 1, pp. 74–80, Jan. 2014, https://doi.org/10.1111/jace.12600.
12. A. Marzouki *et al.*, "New approach for designing bulk multiferroic composites made of two perovskite oxides with enhanced direct magnetoelectric coupling," *Scr. Mater.*, vol. 194, pp. 5–7, Mar. 2021, https://doi.org/10.1016/j.scriptamat.2020.113673.
13. M. Yao *et al.*, "Great multiferroic properties in BiFeO3/BaTiO3 system with composite-like structure," *Appl. Phys. Lett.*, vol. 122, no. 15, Apr. 2023, https://doi.org/10.1063/5.0139017.
14. M. Yao *et al.*, "Grain size and piezoelectric effect on magnetoelectric coupling in BFO/PZT perovskite-perovskite composites," *J. Alloys Compd.*, vol. 948, p. 169731, Jul. 2023, https://doi.org/10.1016/j.jallcom.2023.169731.
15. J. Chen, L. Hu, J. Deng, and X. Xing, "Negative thermal expansion in functional materials: controllable thermal expansion by chemical modifications," *Chem. Soc. Rev.*, vol. 44, no. 11, pp. 3522–3567, 2015, https://doi.org/10.1039/C4CS00461B.
16. T. C. Lu, J. Yang, Z. Suo, A. G. Evans, R. Hecht, and R. Mehrabian, "Matrix cracking in intermetallic composites caused by thermal expansion mismatch," *Acta Metall. Mater.*, vol. 39, no. 8, pp. 1883–1890, Aug. 1991, https://doi.org/10.1016/0956-7151(91)90157-V.
17. J. Zhou, H. He, Z. Shi, G. Liu, and C.-W. Nan, "Dielectric, magnetic, and magnetoelectric properties of laminated PbZr0.52Ti0.48O3/CoFe2O4 composite ceramics," *J. Appl. Phys.*, vol. 100, no. 9, Nov. 2006, https://doi.org/10.1063/1.2358191.

18. L. K. Pradhan, R. Pandey, R. Kumar, and M. Kar, "Lattice strain induced multiferroicity in PZT-CFO particulate composite," *J. Appl. Phys.*, vol. 123, no. 7, Feb. 2018, doi: 10.1063/1.5008607.
19. Z. Manzoor, A. Khalid, G. M. Mustafa, S. M. Ramay, S. Naseem, and S. Atiq, "Magnetoelectric coupling caused by strain mediation in hetero-structured spinel-perovskite multiferroic composites," *J. Magn. Magn. Mater.*, vol. 500, p. 166409, Apr. 2020, https://doi.org/10.1016/J.JMMM.2020.166409.
20. J. D. Bucci, B. K. Robertson, and W. J. James, "The precision determination of the lattice parameters and the coefficients of thermal expansion of BiFeO 3," *J. Appl. Crystallogr.*, vol. 5, no. 3, pp. 187–191, Jun. 1972, https://doi.org/10.1107/S0021889872009173.
21. B. Malič, H. Razpotnik, J. Koruza, S. Kokalj, J. Cilenšek, and M. Kosec, "Linear thermal expansion of lead-free piezoelectric K0.5Na0.5NbO3 ceramics in a wide temperature range," *J. Am. Ceram. Soc.*, vol. 94, no. 8, pp. 2273–2275, Aug. 2011, https://doi.org/10.1111/j.1551-2916.2011.04628.x.
22. A. Ndayishimiye, S. H. Bang, C. J. Spiers, and C. A. Randall, "Reassessing cold sintering in the framework of pressure solution theory," *J. Eur. Ceram. Soc.*, vol. 43, no. 1, pp. 1–13, Jan. 2023, https://doi.org/10.1016/J.JEURCERAMSOC.2022.09.053.
23. Y. Ji *et al.*, "Cold sintered, temperature-stable CaSnSiO5-K2MoO4 composite microwave ceramics and its prototype microstrip patch antenna," *J. Eur. Ceram. Soc.*, vol. 41, no. 1, pp. 424–429, Jan. 2021, https://doi.org/10.1016/J.JEURCERAMSOC.2020.08.053.
24. D. Wang *et al.*, "Direct Integration of Cold Sintered, Temperature-Stable Bi2Mo2O9-K2MoO4 Ceramics on Printed Circuit Boards for Satellite Navigation Antennas," *J. Eur. Ceram. Soc.*, vol. 40, no. 12, pp. 4029–4034, Sep. 2020, https://doi.org/10.1016/J.JEURCERAMSOC.2020.04.025.
25. J. Guo, S. S. Berbano, H. Guo, A. L. Baker, M. T. Lanagan, and C. A. Randall, "Cold Sintering Process of Composites: Bridging the Processing Temperature Gap of Ceramic and Polymer Materials," *Adv. Funct. Mater.*, vol. 26, no. 39, pp. 7115–7121, 2016, https://doi.org/10.1002/adfm.201602489.
26. X. Zhao, J. Guo, K. Wang, T. Herisson De Beauvoir, B. Li, and C. A. Randall, "Introducing a ZnO-PTFE (Polymer) Nanocomposite Varistor via the Cold Sintering Process," *Adv. Eng. Mater.*, vol. 20, no. 7, p. 1700902, Jul. 2018, https://doi.org/10.1002/adem.201700902.
27. H. Zubairi, F. Hussain, S. Sheikh, A. A. Shaikh, D. Wang, and I. M. Reaney, "Comparative study of cold assisted and conventional sintering of (1-2x) K0.5Na0.5NbO3-xBaTiO3-xBiFeO3 multiferroic ceramics," *Mater. Sci. Eng. B*, vol. 296, p. 116632, Oct. 2023, https://doi.org/10.1016/j.mseb.2023.116632.
28. S. Salmanov *et al.*, "Impact of transient liquid phase on the cold sintering of multiferroic $BiFeO_3$," *UNDER Rev. J. - Eur. Ceram. Soc.*, 2024.
29. K. Tsuji, Z. Fan, S. H. Bang, S. Dursun, S. Trolier-McKinstry, and C. A. Randall, "Cold sintering of the ceramic potassium sodium niobate, (K0.5Na0.5) NbO3, and influences on piezoelectric properties," *J. Eur. Ceram. Soc.*, vol. 42, no. 1, pp. 105–111, Jan. 2022, https://doi.org/10.1016/j.jeurceramsoc.2021.10.002.
30. S. Salmanov *et al.*, "Structure and electrical properties of cold-sintered strontium-doped potassium sodium niobate," *J. Eur. Ceram. Soc.*, vol. 43, no. 16, pp. 7516–7523, Dec. 2023, https://doi.org/10.1016/J.JEURCERAMSOC.2023.07.069.
31. M. Makarovic *et al.*, "Tailoring the electrical conductivity and hardening in BiFeO3 ceramics," *J. Eur. Ceram. Soc.*, vol. 40, no. 15, pp. 5483–5493, Dec. 2020, https://doi.org/10.1016/j.jeurceramsoc.2020.06.037.
32. J. Hreščak, B. Malič, J. Cilenšek, and A. Benčan, "Solid-state synthesis of undoped and Sr-doped K0.5Na0.5NbO3," *J. Therm. Anal. Calorim.*, vol. 127, no. 1, pp. 129–136, Jan. 2017, https://doi.org/10.1007/s10973-016-5615-3.
33. A. Jabr, J. Fanghanel, Z. Fan, R. Bermejo, and C. Randall, "The effect of liquid phase chemistry on the densification and strength of cold sintered ZnO," *J. Eur. Ceram. Soc.*, vol. 43, 2023, https://doi.org/10.1016/j.jeurceramsoc.2022.11.071.
34. A. Włódarkiewicz, M. E. Costa, and P. M. Vilarinho, "The dissolution of potassium sodium niobate (KNN) in aqueous media towards sustainable electroceramics sintering," *Mater. Des.*, vol. 233, p. 112169, Sep. 2023, https://doi.org/10.1016/J.MATDES.2023.112169.
35. S. H. Han *et al.*, "Synthesis and characterization of multiferroic BiFeO3 powders fabricated by hydrothermal method," *Ceram. Int.*, vol. 36, no. 4, pp. 1365–1372, May 2010, https://doi.org/10.1016/j.ceramint.2010.01.020.
36. A. F. Mark, M. Castillo-Rodriguez, and W. Sigle, "Unexpected plasticity of potassium niobate during compression between room temperature and 900°C," *J. Eur. Ceram. Soc.*, vol. 36, no. 11, pp. 2781–2793, Sep. 2016, https://doi.org/10.1016/j.jeurceramsoc.2016.04.032.
37. M. Höfling *et al.*, "Large plastic deformability of bulk ferroelectric KNbO3 single crystals," *J. Eur. Ceram. Soc.*, vol. 41, no. 7, pp. 4098–4107, Jul. 2021, https://doi.org/10.1016/J.JEURCERAMSOC.2021.02.023.

38. K. Nakagawa, M. Iwasaki, Z. Fan, J. I. Roscow, and C. A. Randall, "The unusual case of plastic deformation and high dislocation densities with the cold sintering of the piezoelectric ceramic K0.5Na0.5NbO3," *J. Eur. Ceram. Soc.*, vol. 43, no. 9, pp. 4015–4020, Aug. 2023, https://doi.org/10.1016/J.JEURCERAMSOC.2023.02.057.
39. D. Kuscer *et al.*, "Evolution of phase composition and microstructure of sodium potassium niobate –based ceramic during pressure-less spark plasma sintering and post-annealing," *Ceram. Int.*, vol. 45, no. 8, pp. 10429–10437, 2019, https://doi.org/10.1016/j.ceramint.2019.02.102.

Arrived: 29. 04. 2024
Accepted: 06. 08. 2024